

# Crackling Noise, Power Spectra and Disorder Induced Critical Scaling

A. Travesset, R.A. White, and K.A. Dahmen  
Loomis Laboratory, University of Illinois at Urbana  
61801, Urbana, IL, USA

## Abstract

Crackling noise is observed in many disordered non-equilibrium systems in response to slowly changing external conditions. Examples range from Barkhausen noise in magnets to acoustic emission in martensites to earthquakes. Using the non-equilibrium random field Ising model, we derive universal scaling predictions for the dependence of the associated power spectra on the disorder and field sweep rate, near an underlying disorder-induced non-equilibrium critical point. Our theory applies to certain systems in which the crackling noise results from avalanche-like response to a (slowly) increasing external driving force, and is characterized by a broad power law scaling regime of the power spectra. We compute the critical exponents and discuss the relevance of the results to experiments.

# 1 Introduction

Many non-equilibrium physical systems ranging from disordered ferromagnets to superconducting vortices [1], to martensitic shape-memory alloys [2, 3, 4, 5], to earthquakes, exhibit crackling noise[6] in response to smoothly varying external conditions (driving force). While it is not at all obvious that these systems should show similar properties, it is observed that these and other examples in nature exhibit power law scaling of the noise statistics over many decades. The exponents observed in these systems fall into distinct universality classes: Barkhausen noise observed in disordered ferromagnets exhibits power law scaling in the power spectrum (PS)

$$P(\omega) \sim \omega^{-1/\sigma\nu z} , \quad (1)$$

for large frequencies  $\omega$ , with a universal exponent  $1/\sigma\nu z$  that does not depend on the microscopic details, but only on a few basic properties such as symmetries, dimensions, range of interaction, etc. Since universal power law characteristics are often associated with systems at or near an underlying critical point, models with critical points have been suggested to understand the origin of the observed universality.

Barkhausen noise, the characteristic crackling noise associated with the motion of magnetic domain walls in a ferromagnet as the external magnetic field is slowly varied, has enjoyed a significant amount of experimental and theoretical attention in the past decade because it is a particularly simple and experimentally readily accessible example of systems with crackling noise. Models for Barkhausen noise in soft ferromagnets usually model the motion of one (or few) domain walls, while other models, presumably for Barkhausen noise in hard (strongly disordered) magnets model the collective behavior of many interacting domain walls. While the former is marked by long range ferromagnetic interactions which cause the system to “self tune” to the domain wall depinning transition [7] the latter is not self tuned and requires a different mechanism to explain scaling. This mechanism comes in the form of a disorder induced critical point found in the zero temperature, random field Ising model (RFIM) [8, 9] studied far from thermal equilibrium [10]. In this paper we investigate the power spectra (PS) of “Barkhausen noise” in the zero temperature non-equilibrium RFIM and subsequent scaling relations near the disorder induced critical point. Many of the methods will be applicable to other systems with crackling noise [6], arising from the system’s proximity to an underlying non-equilibrium critical point. Within

the RFIM the pulses of the Barkhausen signal are understood as collective events (dubbed avalanches) in which many magnetic domains (spins) flip in time as the external field is slowly ramped up or down. The properties of the Barkhausen signal and corresponding scaling relations are then equivalent to the statistical properties of the avalanches which are obtained by virtue of the system's proximity to a critical point.

The association of an avalanche in the RFIM with a pulse in the Barkhausen signal presents some practical complications in many experimental systems: background noise and finite field sweep rates lead to merging avalanches and ambiguous definitions of pulses. It therefore seems best to use spectral tools [11, 12] to analyze the pulse train as a whole, rather than, say, trying to extract pulse time, or pulse size distributions. The Power Spectra (PS) that will be studied in this paper is defined as the absolute amplitude square of the Fourier Transform of the voltage time series  $V(t)$ . The voltage  $V(t)$  obtained in Barkhausen noise measurements is the voltage induced in a pickup coil as a function of time  $t$ . The signal  $V(t)$  is proportional to the change in magnetization during the microscopic time interval from  $t$  to  $t + \Delta t$ , where  $\Delta t$  is the time it takes a single spin to flip. An alternative and very useful approach to the study of Barkhausen noise at finite sweep rate is provided by the ABBM model [13], which is similar to the mean field approximation of the RFIM. As we will see, for both the ABBM model and the RFIM the high frequency scaling behavior of the PS is independent of the sweep rate and scales with a universal exponent  $1/(\sigma\nu z)$  having a value of 2 within the ABBM model and becomes around 1.77 within the RFIM.

The organization of the paper is as follows. In section 2 we define the zero temperature, non-equilibrium RFIM and review previous results on the scaling behavior of the avalanche size distribution and magnetic hysteresis curves near the underlying disorder induced critical point for an adiabatically slowly increased external magnetic field. In section 3 we introduce the PS, and give scaling predictions for the PS as a function of the amount of disorder near the critical point, again for the adiabatic case. In section 4 we generalize the results on the PS to the case where the external field is swept at a finite rate and give results for the expected critical exponents obtained from Widom scaling collapses of the numerical simulation results. In section 5 an application of the PS to detect lack of causality in the order of spin flips during an avalanche is presented. Finally, in section 6 we summarize the results obtained and discuss related questions to be addressed in the future.

## 2 Hysteresis Modeled with Ising Spins

In the zero-temperature RFIM magnetic domains are represented by Ising spins ( $s_i = \pm 1$ ) on a hyper-cubic  $d$ -dimensional lattice. Spins interact ferromagnetically with their nearest neighbors with a strength  $J$ , and are subjected to a homogeneous external field  $H(t)$ . Structural disorder is included by a quenched random field  $h_i$  at each lattice site, with a Gaussian distribution

$$\rho(h_i) = \frac{1}{2\pi R} e^{-\frac{h_i^2}{2R^2}}, \quad (2)$$

where  $R$  parametrizes the strength of the disorder. Spins interact with an Ising Hamiltonian

$$\mathcal{H} = -J \sum_{\langle i,j \rangle} s_i s_j - \sum_i (H + h_i) s_i \quad (3)$$

The notation  $\langle \rangle$  implies summation over nearest neighbor pairs only. The temperature is set to zero and each spin is aligned with its local effective field  $h_i^{\text{eff}}$ , defined by

$$h_i^{\text{eff}} = J \sum_{j \in \langle i \rangle} s_j + H + h_i, \quad (4)$$

where  $\langle i \rangle$  denotes the nearest neighbors of site  $i$ . The system is studied far from thermal equilibrium, *i.e.* it is typically *not* in the ground state.

A dynamics is introduced into the system as follows: Initially the external magnetic field is at  $-\infty$ , so that all spins are pointing down ( $s_i = -1$  for all  $i = 1, \dots, N$ ). The magnetic field is then slowly increased. The effective field  $h_i^{\text{eff}}$  at each site is computed. If  $h_i^{\text{eff}}$  at site  $i$  changes sign, the corresponding spin  $s_i$  at that site is flipped. A spin flip may trigger neighboring spins to flip as well, thus leading to an avalanche of spin flips, which is the analogue of a Barkhausen pulse in real magnets.

In this paper, the external field will be ramped up and down at a constant rate

$$\Omega \equiv \frac{dH}{dt}. \quad (5)$$

## 3 The Adiabatic Limit

The zero sweep rate limit  $\Omega \rightarrow 0$  is the adiabatic limit. In this limit the external magnetic field is kept fixed during an avalanche. Only after the

avalanche has come to a halt, the external field is increased until it triggers the next avalanche. Combined analytical [10] and numerical approaches [14] have shown that in this case there is a *disorder driven* dynamical phase transition at a critical disorder  $R_c$  ( $R_c = 2.16$  in three dimensions, for the RFIM with nearest neighbor interactions and Gaussian disorder, in units of the exchange coupling  $J$ ), separating a low disorder regime ( $R < R_c$ ) characterized by hysteresis loops with a macroscopic jump ( $\Delta M$ ) in the magnetization  $M$ , from a high disorder regime ( $R > R_c$ ), in which the hysteresis loops look smooth, see Fig. 1. Here the magnetization is defined as  $M \equiv (\sum_{i=1}^N s_i)/N$ , where  $N = L^d$  is the total number of spins in the system,  $L$  its linear size and  $d$  the dimension. The simulation results reported in this paper are exclusively for  $d = 3$ .

$\beta$	$1/\sigma$	$\tau$	$\beta\delta$	$\nu$	$H_c$	$M_c$
0.035(30)	4.20(30)	1.60(6)	1.8(2)	1.4(2)	1.435(4)	0.9(1)

Table 1: Critical exponents and critical fields defined in the text, obtained from simulations of the adiabatic case in  $d = 3$ . The values of  $H_c$  and  $M_c$  are not universal. Values quoted correspond to a RFIM with n.n interactions and with a Gaussian distribution of random fields. From [15].

The jump  $\Delta M$  in the magnetization for  $R < R_c$  scales to zero as

$$\Delta M \sim (R_c - R)^\beta, \quad (6)$$

where  $\beta$  is a universal prediction of the model, table 1. At the critical disorder ( $R = R_c$ ) each branch of the saturation hysteresis loop has one point ( $M_c(H_c)$ ) where the slope diverges,  $dM/dH(H_c) \rightarrow \infty$ : near that point the magnetization is described by a power law of the form

$$|M(H) - M_c| \sim |H - H_c|^{1/\delta} \quad (7)$$

where  $\delta$  is another universal prediction for experiments (table 1).

The apparently smooth parts of the hysteresis loops really consist of many microscopic steps not resolved in Fig. 1. These steps are the avalanches of spin flips, in analogy to Barkhausen pulses in real materials. For  $R > R_c$  the distribution of avalanche sizes  $D(S, R, H)$  (which is proportional to the probability to observe an avalanche of  $S$  spin flips at disorder  $R$  and external field  $H$  in response to a small increase in  $H$ ) scales as

$$D_{int}(S, R, H) \sim S^{-\tau} \bar{\mathcal{D}}_+(S^\sigma r, h/r^{\beta\delta}), \quad (8)$$

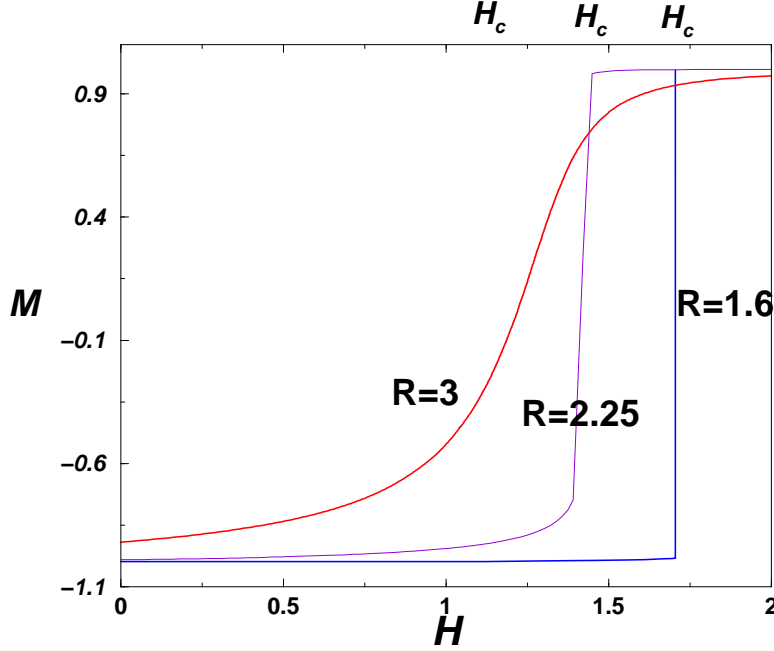


Figure 1: Right branches of hysteresis loops (for increasing  $H$ ) for high disorder  $R = 3$ , close to critical disorder  $R = 2.25$  and low disorder  $R = 1.6$ . Results are for  $L = 200$  at  $\Omega = 10^{-6}$ .

with  $r \equiv (R - R_c)/R_c$ ,  $h \equiv (H - H_c)/H_c$ , and  $\bar{\mathcal{D}}_+$  is a *universal scaling function* [16]. There are similar scaling forms for the avalanche correlation function, the cluster correlation function, and other quantities [16]. The correlation length  $\xi$  scales as the diameter of the largest avalanche of the power law scaling regime of  $D(S, R, H)$ :

$$\xi(r, h) \sim r^{-\nu} \Xi(h/r^{\beta\delta}) , \quad (9)$$

where  $\Xi$  is a universal scaling function [16]. Values for the exponents are given in table 1. Interestingly, numerical simulations indicate that the “critical region” is remarkably large: almost 3 decades of power law scaling in the avalanche size distribution remain when measured at a disorder  $R$  that is 40% away from the critical point. At 2% away one extrapolates seven decades of scaling [16]. This may explain why in many experiments it does not even seem to be necessary to tune the disorder to see the critical power law scaling

over several decades: the samples used may just fall into this large critical region.

### 3.1 Power Spectra

Each avalanche, or Barkhausen pulse, has an internal structure reflecting its evolution with time, see Fig. 2. We denote with  $V(t)$  either the voltage measured in a Barkhausen noise experiment, or the number of spins triggered in our model during the same microscopic time interval of length  $\Delta\tau$ , which is the time it takes a single spin to flip. In our model we set  $\Delta\tau = 1$ . The PS is defined as the amplitude square of the Fourier Transform of the voltage

$$P(\omega) = \left| \sum_{t=t_0}^{t_0+T} e^{i\omega t} V(t) \right|^2. \quad (10)$$

There is some freedom in choosing the initial time  $t_0$  and the total duration of the transform  $T$ . We will provide concrete criteria to fix these parameters.

In the strict adiabatic limit ( $\Omega = 0$ ), avalanches are separated in time by an infinite time, and therefore, only the PS of an isolated avalanche may be rigorously defined. The PS spectra may be defined from the following limiting process: The frequency  $\Omega_A$  is defined as the largest sweep-rate such that no two avalanches overlap in time. The frequency  $\Omega_A$  will be finite in a finite system and will approach zero with increasing volume. The adiabatic limit can then be defined as the infinite volume result of the PS as computed with the sweep rate  $\Omega_A$ . A general scaling form for the PS in the adiabatic case may be derived from generalizing the result of Kuntz and Sethna [17] to the present situation

$$P(\omega, h, r, L) \sim \omega^{-1/\sigma\nu z} \mathcal{F}(\omega^{-1/(\nu z)} r, h/r^{\beta\delta}, Lr^\nu) L^d |\Delta M|, \quad (11)$$

where  $\Delta M \equiv M(t_0 + T) - M(t_0)$ . It was found in [17], that at criticality, for  $\tau < 2$  (as in the RFIM at critical field and disorder),  $P(\omega) \sim \omega^{-1/\sigma\nu z}$  for large  $\omega$ . On the other hand, for  $\tau > 2$ , at the critical point, for large  $\omega$ , one finds  $P(\omega) \sim \omega^{(\tau-3)/\sigma\nu z}$ . The scaling form  $\mathcal{F}$  is therefore more conveniently split into two contributions [17] so that the general form for the PS becomes

$$P(\omega, h, r, L) \sim \omega^{-1/\sigma\nu z} \mathcal{F}_1(\omega^{-1/(\nu z)} r, h/r^{\beta\delta}, Lr^\nu) L^d |\Delta M| + \omega^{(\tau-3)/\sigma\nu z} L^{\frac{\tau-2}{\sigma\nu z}} \mathcal{F}_2(\omega^{-1/(\nu z)} r, h/r^{\beta\delta}, Lr^\nu) L^d |\Delta M| \quad (12)$$

where  $\mathcal{F}_1$  and  $\mathcal{F}_2$  are universal scaling functions, which become finite for large frequencies.

## 4 Finite Field Sweep rate

The above scaling forms were all obtained for zero field sweep rate. In the following section we take into account that in experiments typically the external magnetic field is ramped up and down with a constant finite sweep rate  $\Omega \equiv dH/dt > 0$ . In order to compare sweep rates at different volume

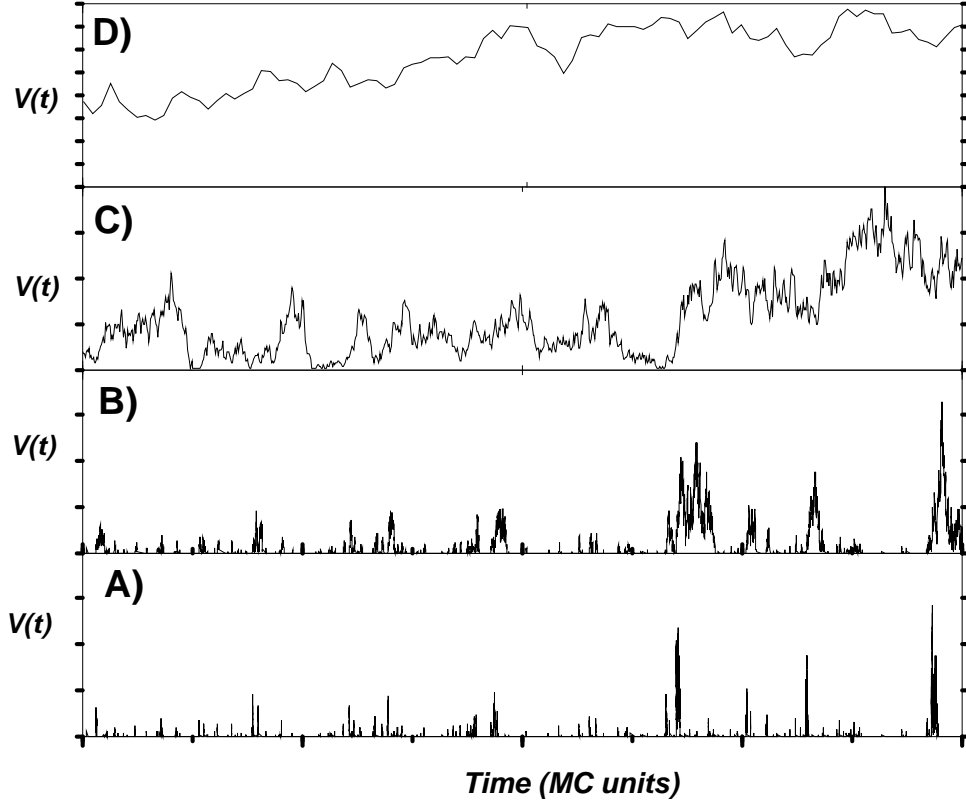


Figure 2: Time series for the noise signal in a ferromagnetic system. This corresponds to a time series for sweep rates of increasing magnitude from A to D.

sizes, it is convenient to define

$$\Omega = \frac{v}{N}, \quad (13)$$

where  $N$  is the number of spins in the actual system and  $v$  defines a size independent sweep rate. In contrast to the adiabatic case (  $\Omega \rightarrow 0$  ) where



the external magnetic field is kept fixed during an avalanche, at finite field sweep rate it can trigger new avalanches before currently running ones have petered out, see Fig. 2.

Interestingly, the Barkhausen noise time series at relatively fast sweep rates  $\Omega$  (as in case *D* in Fig. 2, where basically no separate avalanches can be identified since most individual avalanches overlap in time) has the same PS as the low driving sweep rate cases *A*, *B* or *C*, at least for high frequencies  $\omega$ , and therefore results in the same high frequency noise scaling exponents. This highlights the usefulness of the power spectra: it allows to characterize Barkhausen noise in situations where individual avalanches cannot be observed separately.

To anticipate the effect of finite sweep rate we note the general form of the power spectra of an ensemble of independent pulses given in [18] where it is assumed that there are no size correlations between pulses:

$$P_{total}(\omega) = a(H)\Omega \left[ \langle P(\omega) \rangle + 2 |\langle \Phi(\omega) \rangle|^2 \text{Re} \left( \frac{\int_0^\infty D(\Delta T) e^{i\omega\Delta T} d\Delta T}{1 - \int_0^\infty D(\Delta T) e^{i\omega\Delta T} d\Delta T} \right) \right], \quad (14)$$

where  $\langle \rangle$  is the average over all the individual pulses,  $\Phi(\omega)$  is the Fourier transform of an individual pulse and  $D(\Delta T)$  is the distribution of time intervals between independent, successive nucleation events (*i.e.* spin flips that in the adiabatic limit would be triggered only by an increase in the external magnetic field rather than some neighboring spin flips).  $a(H)$  is the number of nucleation events per unit field increase, yielding  $a(H)\Omega\mathcal{T}$  nucleations in a time span  $\mathcal{T}$ .

As shown in Fig. 3, for the RFIM with only n.n. interactions  $D(\Delta T)$  is Poissonian, leaving the second term in brackets zero. Hence the resulting PS is simply proportional to the sum of the individual PS. This holds as long as any simultaneously propagating collective events do not overlap in *space* (otherwise the pulses can no longer be considered independent [19]). Conveniently, this implies that the PS can be used to determine many scaling properties of the simultaneously propagating adiabatic avalanches at high sweep rates.

It is important to note here that the introduction of long range (anti-ferromagnetic) dipole-dipole interactions, as present in soft magnetic materials, would lead to distinctly non-Poissonian  $D(\Delta T)$  which results in a nontrivial sweep rate dependence in  $P_{tot}(\omega)$ . We leave a detailed study of this dependence for the future. The results of this paper are expected to

### Evidence of statistical independence of nucleations

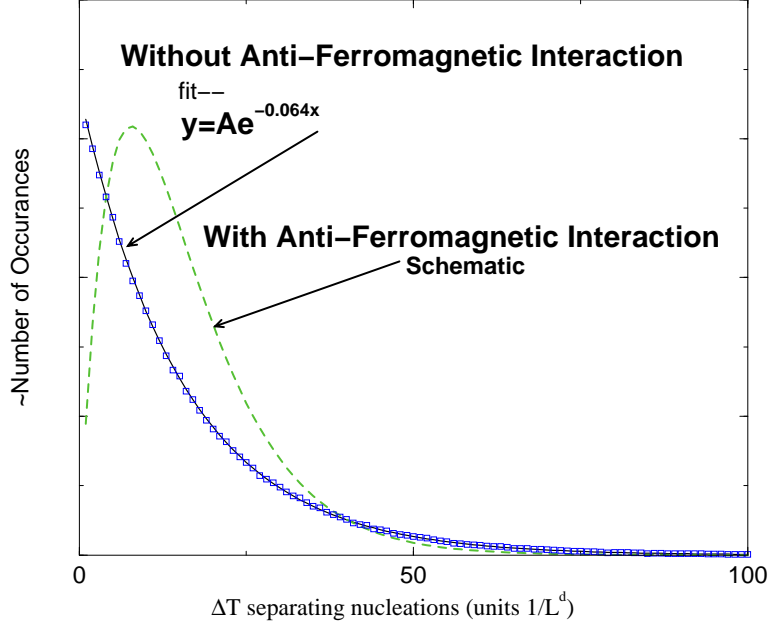


Figure 3: Plot of the distribution of time intervals  $\Delta T$  separating successive nucleation events. The continuous line is a fit to a Poissonian distribution. For comparison, a schematic figure for an anti-ferromagnetic interaction is shown.

apply to hard magnets and other systems, in which long range dipolar fields are negligible due to sample geometry and other factors.

#### 4.0.1 The determination of $H_c$

Before testing the above scaling relations Eq. 12, and Eq. 14, we first need a criteria to pick up a sensible initial time  $t_0$  and total length  $T$  of the Fourier transformed Barkhausen train to compute the PS (see Eq. 10). In order to apply Eq. 12 at the critical field ( $h = 0$ ) we choose the Fourier transformed interval such that

$$H_c \in [H(t_0), H(t_0 + T)] . \quad (15)$$

Furthermore, in order to have sensible statistics, one would like to include as many spins flips as possible in the time series, while keeping the deviation

from  $H_c$  small enough so that Eq. 12 with  $h = 0$  is still applicable. We typically choose the intervals such that  $h \equiv (H - H_c)/H_c < 0.05$ . This way, it is found that a reasonable fraction of the spins are included in the time series and the range of recorded events spans all sizes.

#### 4.0.2 How fast is fast?

We now compute the critical sweep-rate  $\Omega_c$ , above which one observes changes of the PS due to spatially overlapping simultaneous events. Since the nucleations of avalanches are random in time (*i.e.* Poisson distributed) Eq. 14 implies that the adiabatic scaling result for  $P(\omega)$  will hold as long as the spin flip order is maintained for the adiabatic avalanches. That is, as long as we are superimposing the adiabatic avalanches to construct the time series we are assured of obtaining a power spectra that is the superposition of the PS of the individual pulses. The flip order begins to change when, during the propagation of an avalanche, new avalanches are triggered within the same volume that the initial avalanche would have eventually covered. The increased sweep-rate leads to “parallel processing” and the avalanche that would have taken  $T$  time steps to complete now takes  $T'$  such that  $T' < T$  for all  $\Omega > \Omega_c(T)$ . The field sweep rate at which the expected number of spins flipped in avalanches triggered within the volume of the primary avalanche is some finite fraction of the primary avalanche size is given for an avalanche of duration  $T$  as [19]

$$\Omega_c(T) = \frac{\xi^{d_f(\tau-2)}}{T} \quad (16)$$

Since the power spectra is a superposition of all the individual avalanches there will not be any change in the PS as long as

$$\Omega < \Omega_c \equiv \frac{\xi^{d_f(\tau-2)}}{T^*} \quad (17)$$

where  $T^*$  is the largest duration observed which scales as  $T^* \sim \xi^z$ . Since  $\xi \sim L$  if  $r^{-\nu} > L$  or  $\xi \sim r^{-\nu}$  if  $r^{-\nu} < L$  the critical field sweep rate has two scaling forms

$$\Omega_c \sim L^{d_f(\tau-2-\sigma\nu z)} \text{ for } \xi \gg L \quad (18)$$

$$\Omega_c \sim \xi^{d_f(\tau-2-\sigma\nu z)} \text{ for } \xi \ll L. \quad (19)$$

We note here that if  $\tau - 2 - \sigma\nu z > -1$ , as is the case in the RFIM, then even if the avalanches are compact, *i.e.*  $d_f = d$ , the onset of sweep rate effects happens at a field sweep rate much faster than the largest sweep rate at which one can still measure separate pulses (since  $\Omega$  is measured in units of  $1/L^d$ ). Fig. 4 confirms the applicability of the adiabatic result to a large range of external sweep rates  $\Omega < \Omega_c$ .

Furthermore even for  $\Omega > \Omega_c$  we can derive a frequency  $\omega_a(\Omega) \equiv \Omega \xi^{d_f(2-\tau)}$  so that for  $\omega > \omega_a(\Omega)$  the power spectra are again described by the adiabatic results [19]. Below this frequency the PS follows a cutoff function as a result of the sweep rate decreasing the duration of the larger avalanches (see Fig. 4). For  $\omega \ll \Omega$  one finds the asymptotic  $\omega \rightarrow 0$  result

$$\lim_{\omega \rightarrow 0} P(\omega) = L^{2d} |M(t_0 + T) - M(T)|^2 \equiv L^{2d} |\Delta M|^2 . \quad (20)$$

Recalling the scaling relation [10]

$$\Delta M \sim r^\beta \mathcal{M}(hr^{-\beta\delta}, Lr^\nu) , \quad (21)$$

near the critical point, in the adiabatic case ( $\Omega \rightarrow 0$  first)

$$\lim_{\omega \rightarrow 0} P(\omega) = L^{2(d-\beta/\nu)} \text{ for } r \rightarrow 0 , h \rightarrow 0. \quad (22)$$

Let us recall that while in [17], the limit of small  $\omega$  is taken after the adiabatic  $\Omega \rightarrow 0$  limit has been performed, in our simulations we will be working at finite sweep rates and therefore, our PS will always satisfy Eq. 20 correctly (with non-zero  $\Delta M$ ). It will be shown, however, that in  $d = 3$  dimensions,  $\beta/\nu$  will be very close to zero and therefore, even the adiabatic limit scales very approximately as  $L^6$ .

#### 4.0.3 Critical exponents

The PS is now obtained from numerical simulations and the scaling prediction Eq. 12 in section 3.1 is used to extract critical exponents. The results presented involve averages over several, usually about 16, disorder realizations.

Besides the external driving frequencies, there are two additional natural frequencies in the system defining the characteristic times of the largest events in the system:

$$\omega_r \equiv \frac{1}{\xi(r)^z} , \quad (23)$$

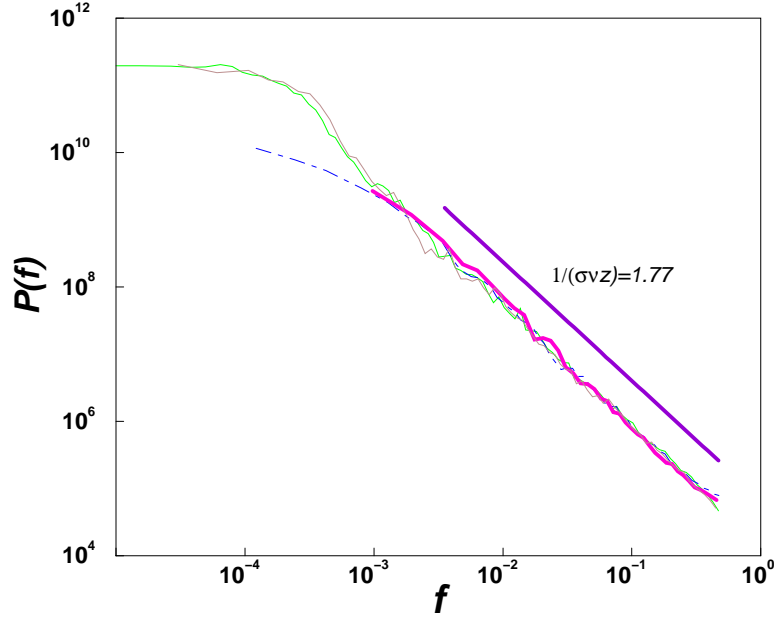


Figure 4: Plot of the PS (for  $f \equiv \frac{\omega}{2\pi}$ ) as a function of  $\Omega$  at  $R_c$  for  $L = 100$ . Result includes  $\Omega = 10^{-9}$  and  $\Omega = 10^{-6}$  (thin solid lines),  $\Omega = 10^{-4}$  (dot-dashed line) and  $\Omega = 10^{-3}$  (wide solid line). The fit  $P(f) \sim f^{-1/(\sigma\nu z)}$  corresponds to  $\Omega = 10^{-9}$  and has been separated for proper visualization.

where  $\xi(r)$  is the correlation length, and

$$\omega_L \equiv \frac{1}{L^z} , \quad (24)$$

where  $L$  is the finite linear size of the system.

For future convenience, we introduce a simple continuous function  $\omega_c$  that asymptotically approaches the values of  $\omega_r$  and  $\omega_L$ , as  $\xi/L \rightarrow 0$  and  $\xi/L \rightarrow \infty$ , respectively:

$$\omega_c \equiv \frac{1 + \xi(r)^z/L^z}{\xi(r)^z} = \omega_r + \omega_L . \quad (25)$$

Other definitions with the same asymptotics can also be used.

In Fig. 5 the PS for  $H$  from a small interval around  $H_c$  is shown as a function of the disorder strength for fixed system size. As the disorder approaches  $R_c$ , the system size  $L$  becomes the characteristic length scale

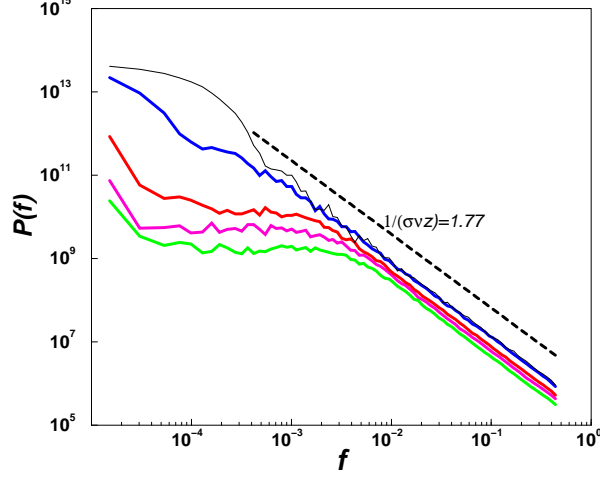


Figure 5: Power Spectra for ( $f = \frac{\omega}{2\pi}$ ) at different disorder values  $R = 2.30$ ,  $R = 2.50$ ,  $R = 2.60$ ,  $R = 2.70$ . The thin line corresponds to  $R = 2.20 < R_c$ , and the dashed line is the fit to  $R = 2.30$  (it has been shifted for proper visualization). Results correspond to  $L = 200$ ,  $\Omega = 10^{-6}$ , and  $H$  in a small interval around  $H_c$  with  $(H - H_c)/H_c < 0.05$ .

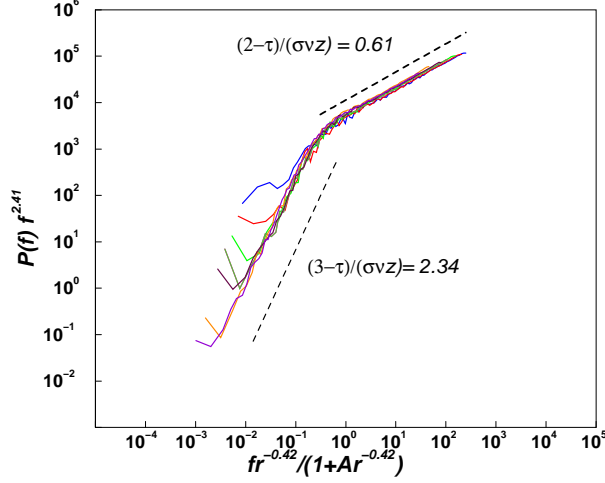


Figure 6: Power Spectra (for  $f = \frac{\omega}{2\pi}$ ) collapse for disorder values  $R = 2.3$  to  $R = 2.7$  at  $L = 200$ ,  $\Omega = 10^{-6}$ , according to Eq. 27. The value of  $A$  is a non-universal parameter dependent on the size of the system  $L$ . ( $A \sim L^z$ ).

of the system implying that  $\omega_L$  takes over  $\omega_r$  as the characteristic cut-off frequency, and one observes a very large region of power law scaling (about four decades for  $L = 200$ ). For larger disorder  $R > R_c$ , it becomes apparent that  $\omega_c \sim \omega_r \sim r^{\nu z}$  in agreement with the behavior suggested in Eq. 12.

At large frequencies  $P(\omega) \sim \omega^{-1/\sigma\nu z}$ , as expected, with

$$1/(\sigma\nu z) = 1.77(4) , \quad (26)$$

where the error bar merely indicates the dispersion around the mean value from the different fits to Eq. 12 corresponding to the different disorder parameters and system sizes considered.

More information can be obtained from a scaling collapse of the PS for different disorders. Setting  $h = 0$  in the adiabatic scaling form Eq. 12 we can make an Ansatz for the specific form of the scaling function  $\mathcal{F}$  to arrive at the scaling form (assuming  $\tau < 2$ , as discussed) for  $\frac{\xi}{L} < 1$ :

$$P(\omega) = \left(\frac{\omega}{\omega_L}\right)^{-\frac{3-\tau}{\sigma\nu z}} \mathcal{Q}\left(\frac{\omega}{\omega_c}\right) |\Delta M| L^{d+1/\sigma\nu} . \quad (27)$$

The factor of  $|\Delta M| L^d$  is a normalization factor resulting from our specific definition of  $P(\omega)$ . Its particular form in the adiabatic case has been given in Eq. 22. The asymptotic behavior of the function  $\mathcal{Q}$  is given by simple power laws (with  $x = \frac{\omega}{\omega_c}$ ):

$$\mathcal{Q}(x) = \begin{cases} x^{\frac{2-\tau}{\sigma\nu z}} & , \quad x \gg 1 \\ x^{\frac{3-\tau}{\sigma\nu z}} & , \quad x \ll 1 \end{cases} , \quad (28)$$

where the scaling for  $x \gg 1$  implies the expected behavior  $\omega^{-1/(\sigma\nu z)}$  at large frequencies. Plugging Eq. 25 and Eq. 28 into Eq. 27, for  $x \ll 1$ , one obtains:

$$P(\omega) \sim \left(\frac{\xi}{L} \left(1 + \left(\frac{\xi}{L}\right)^z\right)\right)^{\frac{3-\tau}{\sigma\nu z}} , \quad \omega \ll \omega_c , \quad (29)$$

*i.e.* the PS becomes independent of the frequency. This is a consequence of the fact that the system is above criticality, there is a minimum cut-off frequency  $\omega_r$ , which corresponds to the finite duration of the largest avalanche in the system, with no characteristic events having larger durations. This result is reflected by the low frequency plateau at large disorder in Fig. 5.

The collapse obtained using the scaling form Eq. 27 is plotted in Fig. 6. For the particular system size shown ( $L = 200$ ), the collapse extends up to

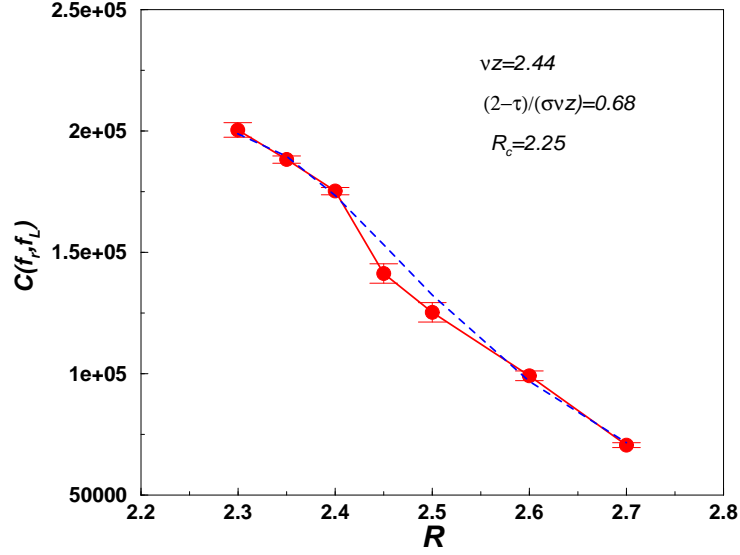


Figure 7: The coefficient  $C(f_r, f_L) \equiv \frac{C(\omega_r, \omega_L)}{(2\pi)^{1/\sigma v z}}$ , see Eq. 31 as a function of disorder  $R$  for  $L = 200$  and  $\Omega = 10^{-6}$  (grey dots). The dashed line corresponds to a fit according to Eq. 31.

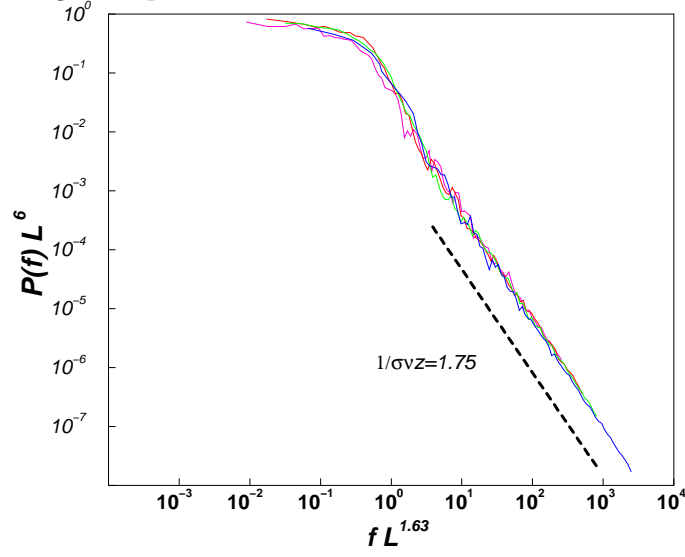


Figure 8: Finite size scaling collapse of Power Spectra (for  $f = \frac{\omega}{2\pi}$ ) at  $R = R_c$  for system sizes  $L = 50$  to  $L = 200$ , ( $L=50,75,100,150,200$ ), collapsed according to Eq. 34.



about five decades and it only fails for very low frequencies that are of order or smaller than the (small) nonzero external sweep rate  $\Omega$  in the simulations.

From the collapse one obtains the critical exponents

$$\frac{1}{\nu z} = 2.38(10) , \quad \frac{3 - \tau}{\sigma \nu z} = 2.41(10) , \quad \frac{2 - \tau}{\sigma \nu z} = 0.61(9) , \quad (30)$$

with error bars estimated as previously.

It is found that  $L^d \Delta M$  is numerically very close to  $L^d$ , and from this and the scaling form Eq. 21 one derives that  $\beta$  is close to zero within the accuracy of our calculation.

Additional information may be obtained by further exploiting the large frequency behavior in Eq. 27,  $\omega \gg \omega_c$ . We can write

$$\begin{aligned} P(\omega) &= C(\omega_r, \omega_L) \omega^{-1/(\sigma \nu z)} \quad \omega \gg \omega_c \\ C(\omega_r, \omega_L) &= \bar{A}(L) \left( \frac{r^{-\nu z}}{1 + (\frac{\xi}{L})^z} \right)^{\frac{2-\tau}{\sigma \nu z}} , \end{aligned} \quad (31)$$

One can fit the coefficient  $C$  for different disorder values (see Fig. 7), where  $L$  and therefore  $\bar{A}(L)$  is a constant). The fit is excellent at the two ends of the curve and becomes slightly inaccurate on the region  $\xi/L \sim 1$ , which is a consequence of the approximation made in selecting the interpolation function for  $\omega_c$  given in Eq. 25. Since the exponents are computed from the two ends, one obtains

$$\frac{1}{\nu z} = 2.44(10) , \quad \frac{2 - \tau}{\sigma \nu z} = 0.68(8) , \quad (32)$$

which provides a cross check of the validity of the results obtained in the collapse. It is also interesting to compute the correlation length

$$\xi(R) = 9.68 \left( \frac{R - R_c}{R_c} \right)^{-1.40} . \quad (33)$$

The large exponent  $\nu \simeq 1.4(1)$  is partly responsible for the large scaling region of the non-equilibrium RFIM [10].

#### 4.0.4 Finite Size Scaling

The analysis of the PS as a function of the linear system size  $L$  at criticality  $r = h = 0$  is also very interesting. From Eq. 12 one derives the adiabatic

scaling form

$$P(\omega)L^{1/(\sigma\nu)+d}|\Delta M| = P(\omega)L^{d-\beta/\nu+1/(\sigma\nu)} = \mathcal{G}(\omega L^z) , \quad (34)$$

with the universal scaling function  $\mathcal{G}(x) \sim 1$  for  $x \rightarrow 0$  and  $\mathcal{G}(x) \sim x^{-1/(\sigma\nu z)}$  for  $x \rightarrow \infty$ . Fig. 8 shows that the data collapse very well to the assumed relation for all the included frequencies (about five decades of scaling for  $L = 200$ ). The resulting exponents are

$$z = 1.63(10) \quad , \quad 1/(\sigma\nu z) = 1.75(6) \quad , \quad \theta/2 + 1/\sigma\nu = 3.0(5) \quad (35)$$

where the exponent relation  $\theta = d - \beta/\nu - 1/(\sigma\nu)$  [10] has been used and the error bars indicate the dispersion from the values obtained as a consequence of disorder fluctuations.

## 4.1 Below $R_c$

### 4.1.1 General Forms

The hysteresis loops of the RFIM below the critical disorder  $R_c$  have a macroscopic jump in the magnetization at a critical field  $H_c(R)$  where many spins flip almost simultaneously in an event that extends over a finite fraction of the system. The jump grows with decreasing disorder. Studying the critical behavior of the RFIM below  $R_c$  gets complicated by the fact that even if the correlation length becomes smaller than the system size, there is always an event which is sensitive to the system size, and in previous studies, large finite size effects have made the analysis at  $R < R_c$  difficult. The PS below but near  $R_c$  for  $\omega > \Omega$  can be collapsed using the scaling form

$$P(\omega) = \phi\left(\frac{\omega/\omega_L}{1 + \omega_r/\omega}\right)|\Delta M|L^{1/(\sigma\nu)+d}. \quad (36)$$

with  $\phi(x) \sim x^{-1/(\sigma\nu z)}$  for  $x \gg 1$ . The latter result states that short-time propagation of the avalanches proceeds in the same way, whether above or below (but close to) the critical disorder. At zero disorder, the PS is a constant:

$$\lim_{R \rightarrow 0} P(\omega) = L^{2d}. \quad (37)$$

According to Eq. 20, this also scales as the limit of the PS for  $R > 0$  for  $\omega \ll \Omega$ . The total duration  $T_{\Delta M}(L, R)$  of the jump in the magnetization

for  $R < R_c$  decreases for decreasing  $R$ . This leads to an increasing cut-off frequency

$$\omega(r, L) \sim \frac{1}{T_{\Delta M}(L, R)} , \quad (38)$$

with  $P(\omega) \sim 1/\omega^{1/(\sigma\nu z)}$  for  $\omega > \omega(r, L)$  and  $P(\omega) \rightarrow CL^{d+1/(\sigma\nu)}|\Delta M|$  with  $C$  a constant, for  $\Omega \ll \omega \ll \omega(r, L)$  and  $P(\omega) \rightarrow L^{2d}$  for  $\omega \ll \Omega$ .

Note that the scaling form Eq. 36 is really a special case of the general form Eq. 12 for  $\tau < 2$  derived above  $R_c$  with different scaling functions  $\mathcal{F}_1$  and  $\mathcal{F}_2$ .

Far below  $R_c$  for very large systems we expect Eq. 36 to be replaced by a scaling form that involves the critical exponents of single interface depinning [8, 9], some of which are very close to the exponents of the critical point studied in this paper (for example,  $\frac{1}{\sigma\nu z}$  is the same within error bars) [17].

For the numerical analysis we note that the general considerations discussed in subsections 4.0.1 and 4.0.2 concerning choosing the interval so that it includes  $H_c(R)$ , its width and the range of sweep rates, applies in the regime below  $R_c$  as well.

#### 4.1.2 Critical Exponents

The first issue we investigate is the large frequency limit, which is described by Eq. 36. In Fig. 9 the results of the PS are plotted for different disorder parameters  $R < R_c$ , for a low sweep rate  $\Omega = 10^{-6}$  and in the adiabatic case ( $\Omega = 0$ ) the fit to the large frequency behavior gives

$$1/(\sigma\nu z) = 1.79(5) , \quad (39)$$

with error bars defined as previously.

Fig. 9 shows very clearly, particularly for the PS at  $R = 1 \ll R_c$ , that for decreasing disorder  $P(\omega)$  tends to a constant over larger and larger regimes  $\omega < \omega(r, L)$ , and consequently the large frequency region where the behavior Eq. 36 holds, shrinks.

Fig. 10 shows a collapse of the PS for different disorders according to Eq.(36) over about six decades of scaling for  $L = 200$ , with the critical exponents

$$\nu z = 2.38(10) , \quad 1/(\sigma\nu z) = 1.77(5) . \quad (40)$$

In contrast to the analysis for  $R$  above  $R_c$ , the analysis below  $R_c$  does not involve the exponent  $\tau$ , related to the distribution of avalanche sizes.

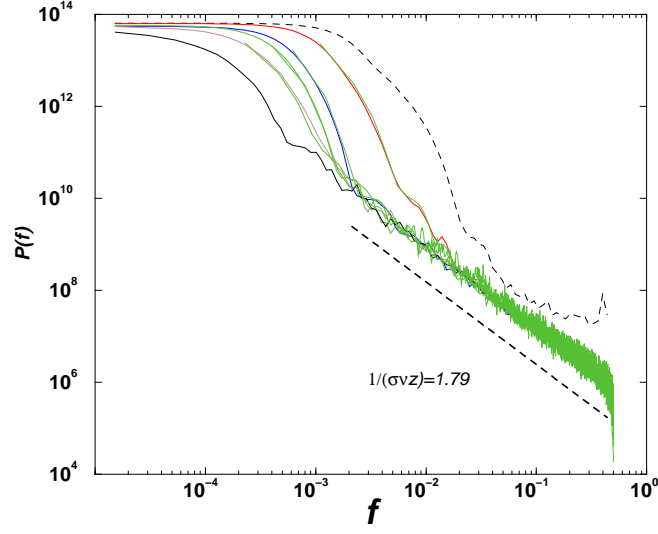


Figure 9: The Power spectra (for  $f = \frac{\omega}{2\pi}$ ) for data below  $R_c$  for  $L = 200$  and disorders between  $R = 2.2$  and  $R = 1.6$ .  $R = 1.0$  is plotted with a thin dotted line, for  $\Omega = 10^{-6}$ . All other curves are plotted for  $\Omega = 10^{-6}$  and  $\Omega = 0$  (adiabatic limit). The fit (straight dashed line) is slightly shifted for proper visualization.

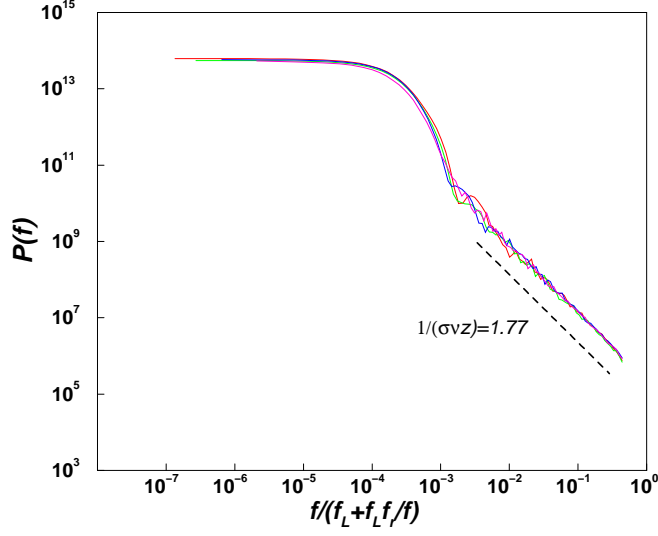


Figure 10: Collapse of the Power spectra (for  $f = \frac{\omega}{2\pi}$ ) for disorders  $R = 2.2$  to  $R = 1.6$ , for  $L = 200$  and  $\Omega = 10^{-6}$ . The data is collapsed according to Eq. 36, and  $f_L \equiv \omega_L/2\pi$  and  $f_r \equiv \omega_r/2\pi$ .

More information below  $R_c$  may be obtained from the region  $\xi(r) \gg L$  where finite size effects dominate. Actually, the PS may be collapsed exactly as in Eq. 34, and the exponents

$$z = 1.63(10) \quad , \quad 1/(\sigma\nu z) = 1.75(6) \quad , \quad (41)$$

follow. Since the PS in this region becomes insensitive to the correlation length  $\xi$ , the results are identical to the ones above  $R_c$ .

## 5 The Interpretation of the Power Spectra

The previous analysis has shown that the PS is sensitive to the causality relations among spins. This point can be made more explicit by considering a different dynamics than the causal dynamics implemented in this paper. Let us consider a standard metropolis dynamics, as if we were introducing temperature into the model. The algorithm is as follows: Spins are randomly selected<sup>1</sup>, and the standard Metropolis (or Glauber) acceptance/rejection check is used to determine whether the spin is to be flipped. Let us recall that since we are considering the temperature to be zero, the proposed move is accepted if the local energy  $E_i \equiv -h_i^{eff} \sigma_i$  of the spin being tested is positive and rejected if it is negative. After  $N$  such attempts to flip randomly chosen spins are performed, the time is increased by one unit.

A spin can only flip when it is selected, and therefore, if that particular spin is not selected by the random update, there will be a delay between the time when it is energetically favorable (which is the time when the spin would be flipped in the causal dynamics) and the time in which the spin actually flips. Spins flipping at earlier times as compared to the causal dynamics may also take place, since the random process may flip a spin seeding an avalanche, and within the same unit of time during the  $N$  attempts before updating the time by one unit, some of the neighbors to this seeding avalanche spin, which become now energetically unstable, may be flipped. Within the causal dynamics those spins would flip at later times.

In Fig. 11 the time series generated from these two dynamics are shown and are extremely close. The PS, however, as shown in Fig. 12, has a different high frequency behavior, and it is clearly sensitive to the different dynamics.

---

<sup>1</sup>since the disorder is itself random, a sequential update has very similar effect as a random one, with very similar PS

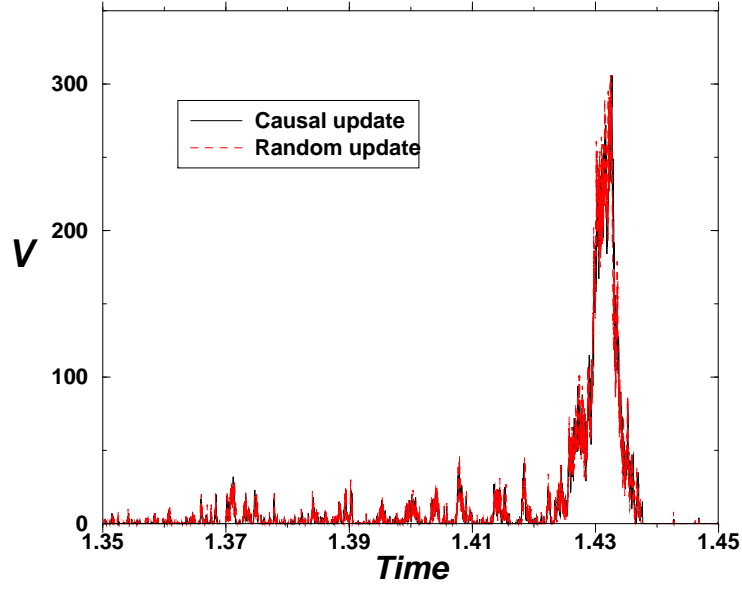


Figure 11: Voltage time series for causal and random updates for a single disorder realization  $R = 2.3$ ).

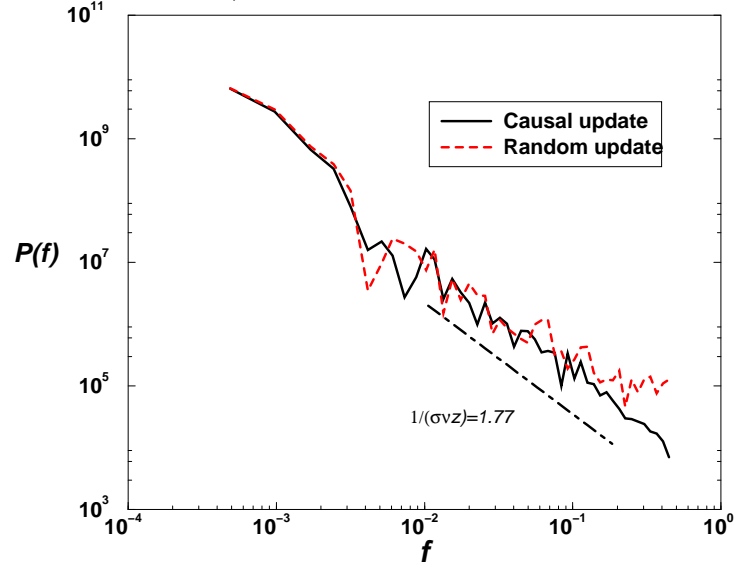


Figure 12: Power Spectra (for  $f = \frac{\omega}{2\pi}$ ) of the previous time series.

Of course, time averages of the magnetization, etc.. will be insensitive to the different dynamics, as is clear from the time series Fig. 11. Observables that show some universality at large frequencies, as is the case for the PS, become sensitive to the different dynamics of spins, even if averaged over several disorder configurations.

The previous remarks are of interest for extensions of the previous study to more general situations, in particular for considering temperature fluctuations when the system is out of equilibrium. Temperature would be naturally introduced into the system by considering Glauber dynamics with random updates, as done in other simulations with Ising spins [20]. Of course any algorithm to study temperature effects should meet the necessary requirements:

- Converge to equilibrium for very slow sweep rates at finite temperature.
- Reduce to the causal dynamics for small temperatures at finite sweep rate.

It follows from our results that the second condition is clearly violated for random updates (or any other update uncorrelated with the dynamics of the system, like a sequential update). The update must be chosen correlated with the dynamics, thus reflecting the causal nature of the events (the avalanches).

## 6 Conclusions

### 6.1 Summary of results

In this paper we have seen that the PS is an extremely valuable observable for the study of collective noise in physical situations where the avalanche picture would no longer be applicable.

Besides its obvious theoretical interest, the PS becomes a powerful practical tool to compute critical quantities. We have computed the following exponents summarized in table 2.

The exponent predictions lie well within the error bars of most Barkhausen noise exponents from experiments quoted in the literature, [6]. Besides, we are able to obtain accurate exponents for the region below  $R_c$ .

The exponent quotes have been deliberately computed at relatively fast sweep rates, see section 4 for a detailed discussion, thus providing conclusive

	Above $R_c$		Below $R_c$	
Quantity	PS	RFIM	PS	RFIM
$1/(\sigma\nu z)$	1.77(3)	1.75(9)	1.79(6)	
$z$	1.63(10)	1.7(2)*	1.63(10)	
$\nu z$	2.38(10)	2.39(40)*	2.38(10)	
$\frac{3-\tau}{\sigma\nu z}$	2.41(10)	2.45(8)*		
$\frac{2-\tau}{\sigma\nu z}$	0.61(9)	0.70(6)*		

Table 2: Exponents computed and the ones known

evidence of the irrelevance of low enough finite field sweep rate for the PS. Finally, it has been shown that the PS is sensitive to the particular dynamics of the spins.

## 6.2 Experiments and Outlook

In Fig. 13 our results are compared to the experiments from [21], corresponding to a *FeSi* sample. Our result for the large frequency dependence of the PS looks more plausible than the exponent  $\frac{1}{\sigma\nu z} = 2$ , suggested by the ABBM model [13]. In [22], the exponent  $\frac{1}{\sigma\nu z} = 2$  is calculated reporting values in the range  $\frac{1}{\sigma\nu z} = 1.5 - 2$ , in agreement with our results, but with a too large uncertainty for a precise comparison. Other experimental determinations in amorphous ribbons of  $Fe_{64}Co_{21}B_{15}$  also seem to favor a value close for  $\frac{1}{\sigma\nu z}$  close to 1.78 [23]. For this particular data we expect that the frequency dependant bump in the PS is due to two things: (1) the presence of long range anti-ferromagnetic (LRAF) interactions which (change the nucleation distribution from Poisson to something more complicated, see section 4, and) affect the low frequency of the power spectra; (2) the fact that the larger avalanches take less time due to “parallel processing” discussed above also diminishes the adiabatic PS in the low frequency regime. While the full details of these effects were not addressed in our current study we are presently investigating effects of LRAF interaction in the RFIM.

In experiments on soft magnetic materials, Barkhausen noise seems to be due to the propagation of a single domain wall, and nucleation of new domains are rare events [7]. Far below  $R_c$ , our model also exhibits domain wall propagation during the macroscopic jump  $\Delta M$  in the hysteresis loop. For small disorder  $R$ , the number of small nucleating events are expected to be negligible, and in this case the PS for the jump at high frequencies should



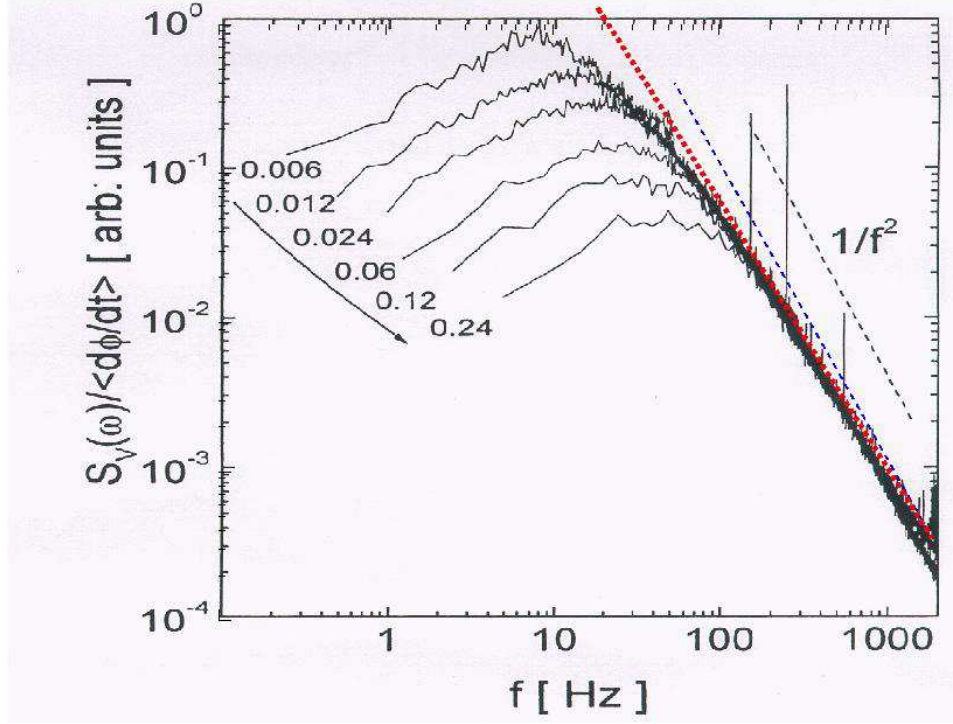


Figure 13: Experimental results from [21]. The dotted line is our prediction 1.78. the dashed line is the result of 2 from the ABBM model [13].

match those of single interface propagation in the absence of LRAF [9, 17] (In some experimental systems the LRAF can be suppressed, for example by applying stress to the sample [23]). It is known that the critical exponents for single interface propagation belong to a different universality class, although the critical exponents characterizing the large frequency limit of the PS turn out to be numerically very close [6, 7]. Therefore, a very detailed study is needed to discriminate between these two regimes (low and near critical disorder) in which the two models apply to the PS.

The main problem for a detailed comparison of the predictions for the disorder induced critical point presented in this paper with the experiments, is the lack of control over the structural disorder in experimental systems. Recent experiments on Co/CoO [24] have shown that in these systems it is possible to control the amount of structural disorder experimentally. If Barkhausen noise is measured in these disorder controlled samples, one could use

the scaling forms derived in this paper and get a very detailed understanding of the universal aspects of hysteresis, including detailed critical exponents near the critical disorder.

Other experimental systems for which such analysis could be extended include acoustic emission in martensitic materials in response to stress or temperature ramping. In fact, the Barcelona group [2, 3, 4, 5] has shown that crackling noise in martensites displays critical scaling in avalanche size distribution and the PS similar to the ones described in this paper for Barkhausen noise, although with different exponents and therefore belonging to a different universality class.

The analysis presented in this paper certainly allows several important applications which we have briefly discussed. First of all, the irrelevance of the sweep rate has very important practical consequences for future calculations since by using a faster sweep rate one can compute the same quantities with less effort. This is an important benefit in situations, as for example the inclusion of temperature, where slow sweep rates are computationally very demanding.

Another important aspect is how long range dipole-dipole interactions may affect the results, a subject briefly discussed in Fig. 3. We hope to report more on that in the near future.

## Acknowledgments

We thank P. Bellon, J.P. Sethna and M.B. Weissman for very claryfing discussions. We thank IBM for a very generous equipment award that made extensive numerical simulations for this work possible. The work by K.A.D, A.T. and R.A.W has been supported by the Materials Computation Center, grant NSF-DMR 99-76550, and NSF grant DMR 00-72783. K.A.D. also gratefully acknowledges support from an A.P. Sloan fellowship.

## References

- [1] F. Nori S. Field, J. Witt and X. Xinheng Ling. *Phys. Rev. Lett.*, 74:1206, 1995.
- [2] E. Vives et al. *Phys. Rev. Lett.*, 72:1694, 1994.
- [3] E. Vives et al. *Phys. Rev. B*, 52:12644, 1995.
- [4] I. Rafols and E. Vives. *Phys. Rev. B*, 52:12651, 1995.
- [5] Ll. Carrillo et al. *Phys. Rev. Lett.*, 81:1889, 1998.
- [6] K. Dahmen J.P. Sethna and C. R. Myers. *Nature*, 2001.
- [7] G. Durin S. Zapperi, P. Cizeau and E.H. Stanley. *Phys. Rev. B*, 58:6353, 1998.
- [8] T. Kinoshita R. Blossey and J. Dupont-Roc. *Physica A*, 248:247, 1998.
- [9] H. Ji and M.O. Robbins. *Phys. Rev. B*, 46:14519, 1992.
- [10] K. Dahmen and J.P. Sethna. *Phys. Rev. B*, 53:14872, 1996.
- [11] M.B. Weissman. *Ann. Rev. Mater. Sci.*, 26:395, 1996.
- [12] J.R. Petta and M.B. Weissman. *Phys. Rev. E*, 57:6363, 1998.
- [13] G. Bertotti B. Alessandro, C. Beatrice and A. Montorsi. *J. Appl. Phys.*, 68:2901, 1990.
- [14] M.C. Kuntz et al. *Computing in Science and Engineering*, 1:73, 1999.
- [15] K. Dahmen O. Perkovic and J.P. Sethna. *Phys. Rev. B*, 59:6106, 1999.
- [16] K. Dahmen O. Perkovic and J.P. Sethna. *Phys. Rev. Lett.*, 75:4528, 1995.
- [17] M. Kuntz and J.P. Sethna. *Phys. Rev. B*, 62:11699, 2000.
- [18] P. Mazzetti. *Il Nuovo Cimento*, 25:1322, 1962.
- [19] R. White and K. Dahmen. in preparation.

- [20] P. Rikvold G. Korniss, C. White and M. Novotny. *Phys. Rev. E*, 63:16120, 2001.
- [21] G. Bertotti B. Alessandro, C. Beatrice and A. Montorsi. *J. Appl. Phys.*, 68:2908, 1990.
- [22] S.L. Queiroz and M. Bahiana. *Phys. Rev. E*, 64:66127, 2001.
- [23] G. Durin and S. Zapperi. *arXiv:cond-mat/0106113*.
- [24] A. Berger et al. *Phys. Rev. Lett.*, 85:4176, 2000.